JBC Papers in Press. Published on August 30, 2012 as Manuscript M111.328781
The latest version is at http://www.jbc.org/cgi/doi/10.1074/jbc.M111.328781

Membrane-induced lever arm expansion allows myosin VI to walk with large and variable step sizes*

Cong Yu[1,5], Jizhong Lou[2,3,5], Jingjing Wu[1], Lifeng Pan[1], Wei Feng[2], and Mingjie Zhang[1,4]

[1]From the Division of Life Science, State Key Laboratory of Molecular Neuroscience, Hong Kong University of Science and Technology, Clear Water Bay, Kowloon, Hong Kong, China;
[2]National Laboratory of Biomacromolecules, Institute of Biophysics, Chinese Academy of Sciences, 15 Datun Road, Beijing 100101, China;
[3]Laboratory of Noncoding RNA, Institute of Biophysics, Chinese Academy of Sciences, 15 Datun Road, Beijing 100101, China; and
[4]Center of Systems Biology and Human Health, Hong Kong University of Science and Technology, Clear Water Bay, Kowloon, Hong Kong, China

[5]: These two authors contributed equally to this work

*Running title: *Lipid membrane-induced lever arm expansion*

To whom correspondence should be addressed: Wei Feng, Institute of Biophysics, Chinese Academy of Sciences, 15 Datun Road, Beijing 100101, China, Tel.: (86) 10-6488-8751; Fax: (86) 10-6488-8237; E-mail: wfeng@ibp.ac.cn ; and Mingjie Zhang, Division of Life Science, Hong Kong University of Science and Technology, Clear Water Bay, Kowloon, Hong Kong, China, Tel.: (852) 2358-8709; Fax: (852) 2358-1552; E-mail: mzhang@ust.hk

Keywords: Myosin VI, lipid membrane, lever arm extension, large-variable step size

---

Background: Myosin VI plays diverse cellular roles ranging from intracellular transport to mechanical anchor.

Results: Myosin VI LAE undergoes reversible, lipid membrane-dependent conformational changes from compact bundle fold to extended rod shape.

Conclusion: LAE functions as "knee-joint" of myosin VI and provides both space and flexibility for stepping.

Significance: The membrane-induced expansion of LAE provides a mechanistic base for myosin VI to walk with large and variable step sizes.

SUMMARY

Myosin VI, the only known minus-ended actin filament-dependent motor, plays diverse cellular roles both as a processive motor and as a mechanical anchor. Even though myosin VI has a short lever arm containing only one "IQ"-motif and a unique insertion for CaM binding, the motor walks with large and variable step sizes of ~30-36 nm. Here, we show that the previously

Copyright 2012 by The American Society for Biochemistry and Molecular Biology, Inc.

Downloaded from www.jbc.org at Hong Kong University of Science & Technology, on September 17, 2012

predicted coiled-coil domain immediately following the "IQ"-motifs (referred to as the lever arm extension, LAE) adopts a stable monomeric, three-helix bundle fold in solution. Importantly, the LAE can undergo reversible, lipid membrane-dependent conformational changes. Upon exposure to lipid membranes, the LAE adopts a partially extended rod shape, and the removal of lipids from the LAE converts it back into the compact helix bundle structure. Molecular dynamics simulations indicate that lipid membrane-binding may initiate unfolding and thereby trigger the LAE expansion. This reversible, lipid membrane-dependent expansion of the LAE provides a mechanistic base for myosin VI to walk with large and variable step sizes.

INTRODUCTION

Originally discovered as a member of the actin filament-associated proteins, myosin VI (Myo6) is the only known molecular motor for the transport of cargoes towards the minus ends of actin filaments (1-2). Myosin VI-mediated reversal transports have been implicated in the control of a variety of cellular processes, such as clathrin-coated/uncoated vesicle-mediated endocytosis, protein secretions at the trans-Golgi network, and asymmetric segregation of cellular components in polarized cells (2-4). Myosin VI also functions as an actin anchor to tether various cellular components to actin filaments for the maintenance of cellular structures including the Golgi complex, the stereocilia of inner-ear hair cells, the leading edges of migrating cells, and the apical junctions of epithelial cells (2,5). In view of the critical functions of myosin VI both as a transporter and as an anchor, it is not surprising that mutations of myosin VI are linked to a number of human diseases, including hereditary deafness and cancers (6-9).

Recent structural and biochemical studies of the myosin VI motor domain together with its neck region (also called the lever arm) have shown that the reverse directionality of myosin VI is conferred by a unique insertion between the motor and the neck region (10-11) (Fig. 1A). The structure of the C-terminal cargo-binding domain (CBD) in complex with its binding domain from the clathrin cargo adaptor Dab2 demonstrates that the cargo-free CBD exists as a monomer in solution, and the binding of Dab2 converts the CBD into a dimer (12). This work, together with a series of biochemistry and cell biology-based studies (13-17), reveals that specific cargoes dictate the conversion of myosin VI from a non-processive monomer to a processive dimer. Regarding myosin VI, another critical question is how the motor can walk on actin filaments with a step size of ~30-36 nm with its unusually short lever arm (18-19). Recent studies uncover that the dimerization of myosin VI can induce the unfolding of a small fragment closely linked to the lever arm to expand its reach (20-21). However, the detailed molecular mechanism governing this unfolding process remains largely unclear. Additionally, it is puzzling how myosin VI with an "unfolded" lever arm transmits its mechanical force generated from its N-terminal motor domain to its cargoes attached at the C-terminal tail.

Myosin VI contains only one "IQ"-motif and a unique insertion (for binding to calmodulin (CaM)) in its lever arm (spanning two-"IQ"-motif length) (Fig. 1A). In contrast, myosin V contains six "IQ"-motifs. Upon binding to CaM, the "IQ"-motifs of each motor form rigid

Downloaded from www.jbc.org at Hong Kong University of Science & Technology, on September 17, 2012

extended α-helices, and these extended α-helices function as the two "legs" that each myosin dimer uses to walk along actin filaments in a hand-over-hand manner (the so-called lever arm hypothesis) (22). Therefore, both the length and the swing angle of the lever arms are directly correlated to the step size of each myosin motor. Consistent with the lever arm hypothesis, myosin V transports cargoes with a large step size of ~36 nm and myosin II (containing two "IQ" motifs) moves on actin filaments with a step size of only ~10 nm (i.e., each "IQ"-motif contribute ~2.5-3 nm of lever arm length) (22-25). However, myosin VI walks along actin filaments with a step size of ~30-36 nm (18-19), which is much greater than what the two-"IQ"-motif of the motor can offer (20), thus challenging the swinging lever arm hypothesis (21,26). Interestingly, a series of recent studies suggest that myosin VI can employ both a hand-over-hand transport manner and an inchworm-like walking mechanism, and the switch between these two mechanisms is controlled by the strain force and ADP (27-29). It has been suggested that the motor may be able to walk with a step size significantly larger by swinging its legs with an angle of ~180° (instead of the ~70° observed for myosin V and myosin II) (11,28,30-32). However, such extreme ~180° "leg-flipping" motion of the motor would still be unable to reach the observed step size of ~36 nm, if the length of the legs is solely determined by its short lever arm (10).

It has been shown that, besides myosin VI's "IQ"-motif-containing lever arm domain, a conserved region of ~80 amino acids immediately following the "IQ"-motif (referred to as the lever arm extension, or LAE) is essential for the large step size of myosin VI (Fig. 1A&B; and refs (33-34)). This LAE, originally predicted to be a rigid coiled-coil, was later suggested to be a rather flexible region, able to provide adequate space for myosin VI to walk with large step sizes (33). The subsequent biochemical and structural studies demonstrated that the LAE, instead of being a coiled-coil dimer or a flexible linker, adopts a compact α-helical globular fold together with the extended single α-helix (SAH) rod immediately C-terminal to it providing additional space required for myosin VI large stepping (34). The crystal structure of the LAE has recently been determined, also confirming the compact helical bundle structure (20). Despite the differences in their structural models, these studies convincingly demonstrated the role of the LAE in the step size of myosin VI, as substitutions of the LAE with either a completely flexible domain or a constrained domain (GCN4 leucine zipper dimer) both shortened the step sizes of the motor (33-34). However, it is conceptually challenging that both myosin VI mutants walk with shortened step sizes, as according to the lever arm hypothesis one would expect the mutant motor with the flexible linker to walk with a larger step size (albeit with potential defects in the mechanical load of the motor).

Here, we determined the solution structure of the LAE by NMR spectroscopy. As expected, the LAE forms a compact three-helix bundle and exists as a stable monomer in solution. Surprisingly, the LAE undergoes reversible, lipid membrane-dependent conformational changes. In the presence of sufficiently high concentrations of membrane liposomes (e.g., a condition comparable to the motor bound to its cargo vesicles), the LAE adopts a partially extended rod conformation composed of three α-helices jointed

Downloaded from www.jbc.org at Hong Kong University of Science & Technology, on September 17, 2012

together by two restrained and retrievable connectors. The steered molecular dynamics (SMD) simulations of the unfolding process reveals the initiation opening site of the LAE, and lipid membranes may function to trigger the unfolding expanding process. Importantly, the removal of lipid liposomes (e.g., a processes equivalent to dissociation of cargo vesicles) from the LAE converts the domain back into its compact three-helix bundle fold conformation. The reversible, cargo vesicle-dependent expansion of the LAE (termed as the expandable "knee joint" of the myosin VI "leg"), together with the previously identified "IQ"-motifs and possibly the SAH rod, provides sufficient space and flexibility for myosin VI to walk on actin filaments with a large and variable step size of ~30-36 nm.

EXPERIMENTAL PROCEDURES

Protein expression and purification

The mouse myosin VI LAE (residue 843-933) fused with an N-terminal His_6-tag was expressed in *E. coli* BL21 (DE3) in its native form. The fusion protein was purified by Ni^{2+}-NTA affinity chromatography followed by size-exclusion chromatography (Superdex-200, GE healthcare). Uniformly isotope-labeled LAE were prepared by growing bacteria in M9 minimal medium using $^{15}NH_4Cl$ as the sole nitrogen source or $^{15}NH_4Cl$ and $^{13}C_6$-glucose (Cambridge Isotope Laboratories Inc.) as the sole nitrogen and carbon sources, respectively. The NMR samples were concentrated to ~0.2 mM (for titration experiments) and ~1 mM (for structural determinations) in 50 mM sodium phosphate, pH 6.5, 2 mM DTT and 2 mM EDTA. All point mutants of the LAE were prepared using PCR-based methods and purified using essentially the same method used for the wild-type protein. The other long forms of the LAE containing the C-terminal SAH region (residues 843-959 and 843-978) were cloned, expressed and purified using the same method used for the wild type LAE.

NMR spectroscopy and structure calculations

NMR spectra were acquired at 30 °C on Varian Inova 500 and 750 MHz spectrometers equipped with a *z*-axis shielded triple resonance probes. Sequential backbone and non-aromatic, non-exchangeable side chain resonance assignments of myosin VI LAE both in aqueous and DPC solutions were achieved by the standard heteronuclear correlation experiments involving HNCO, HNCACB, CBCA(CO)NH, and HCCH-TOCSY using $^{15}N/^{13}C$-labeled samples, and confirmed by 3D ^{15}N-seperated NOESY spectra acquired on ^{15}N-labeled samples (35-36). The side chains of aromatics were assigned by ^{1}H 2D TOCSY and NOESY experiments using unlabeled samples in D_2O (37). Approximate inter-proton distance restraints were derived from 2D ^{1}H-NOESY, 3D ^{15}N-seperated NOESY, and 3D ^{13}C-seperated NOESY spectra. Hydrogen bonding restraints were generated from the standard secondary structure of the protein based on the NOE patterns and backbone secondary chemical shifts. Backbone dihedral angle restraints (ϕ and ψ angles) were derived from the secondary structure of the protein and the backbone chemical shift analysis program TALOS (38). Structures were calculated using the program CNS (39). The protein structure figures were prepared using the programs MOLMOL(40), MOLSCRIPT(41), and PyMOL (http://pymol.sourceforge.net/).

Brain liposome sedimentation assay

Liposome stock was prepared by

Downloaded from www.jbc.org at Hong Kong University of Science & Technology, on September 17, 2012

sonication of bovine lipid extracts (Folch Fraction I, Sigma) in assay buffers. Different concentrations of liposomes were incubated with the purified LAE in the concentration of 40μM and in 50mM Tris, 100mM NaCl, 2mM EDTA and 2mM DTT, pH7.5 buffer for 15 min at room temperature and then centrifuged at 80,000 rpm for 30 min at 4°C in a Beckman TLA100.1 rotor. The supernatants and the pellets were collected and subjected to SDS-PAGE analysis, and proteins were visualized by Coomassie blue staining.

Molecular dynamics simulations

The myosin VI LAE domain structures (bundled or extended) were used as the initial structures for molecular dynamics simulations. For the simulations starting from the bundled conformation, WT or a S909V mutant were simulated. The structures were soaked in a 160 × 64 ×64 $Å^3$ water box, which included 8 Na^+ and 11 Cl^- to neutralize the system. For the simulations starting from the extended conformation, three representative NMR structures were selected and were soaked in 128 × 64 ×72 $Å^3$ water boxes which included 7 Na^+ and 10 Cl^- to neutralize the system.

We also performed simulations to check the potential interactions between the DPC micelle and the LAE. The WT LAE was randomly placed in the vicinity of an initial DPC micelle containing 54 DPC molecules (42), and three different initial configurations were tested, with the LAE αA/αB, αB/αC, and αA/αC interface facing the DPC micelle, respectively. The structures were soaked in a 100×100×100 $Å^3$ water box, with additional Na^+ and Cl^- ions to neutralize the system.

The NAMD package (43) and CHARMM22 all-atom force field (44) were used for energy minimization and molecular dynamics simulations under periodic boundary conditions. A 12-Å cutoff was used for van der Waals interactions and Particle Mesh Ewald summation was used to calculate the electrostatic interactions. Two independent simulations were performed for bundled WT or S909V system. For each simulation, energy was first minimized in multi-steps to avoid any possible clashes. The energy-minimized system was then equilibrated for 6 ns with temperature controlled at 310 K by Langevin dynamics and pressure was controlled at 1 atm by Lagevin piston method. With the equilibrated structures, 20-ns and 36-ns free dynamics simulation was performed for bundled and extended system respectively. The final snapshots of the bundled systems were used as initial conformations for further SMD simulations. The constant-velocity SMD simulations were performed for each system with pulling velocity 0.5 nm/ns and spring constant 70 pN/nm. For the DPC micelle-LAE binding simulations, three independent runs were performed for each initial configuration, and stopped after the separation of the LAE from the DPC micelle or up to 70 ns for the case of the αA/αC interface facing the DPC micelle. All simulation trajectories were analyzed with VMD (45).

Urea denaturation

Purified myosin VI LAE wild type or S909V mutant protein in 50mM Tris, 100mM NaCl, 2mM EDTA and 2mM DTT, pH7.5 buffer containing different concentration of urea were subject to a J-815 spectropolarimeter (Jasco, Tokyo) for CD data collection at room temperature. The concentration normalized ellipticity values at 222 nm were plotted as the function of the urea concentration using the program

Downloaded from www.jbc.org at Hong Kong University of Science & Technology, on September 17, 2012

GraphPad Prism 4. The data were fitted by sigmoidal dose-response (variable slope).

RESULTS

The LAE forms a monomeric globular domain in solution

Given the critical role of the LAE in the step size of myosin VI, we set out to characterize the structural and biochemical properties of the domain (residues 843 to 933). Purified recombinant LAE is stable in solution with a molecular mass of ~11 kD as measured by analytical ultracentrifugation, matching very well with its theoretical monomer mass of ~12 kD (supplemental Fig. S1A). This result confirms the conclusion that the LAE does not form a coiled-coil dimer in solution (33-34). The CD spectrum of the LAE shows that the domain is predominantly α-helical, and the overall folding of the domain is retained even in the presence of 4 M NaCl, indicating that the LAE folds into a highly stable structure in solution (supplemental Fig. S1B). The urea-induced denaturation profile of the domain further supports the stable folding of the LAE in aqueous solution (supplemental Fig. S2A).

Next, we determined the structure of the LAE using NMR spectroscopy. Except for a few residues in the N- and C-termini, the overall structure of the domain is well defined (Fig. 1C&supplemental Table S1). Consistent with our CD-based analysis, the LAE is entirely α-helical and contains three helices (αA-αC) that pack extensively with each other to form a three-helix bundle (Fig. 1D). The crystal structure of the LAE connected with the short lever arm in complex with CaMs has been solved (20), which can be superimposed well with the NMR structure except that the C-terminal half of the first helix (αA) is missing in the crystal structure (supplemental Fig. S3 and see below for details). Each helix of the LAE contains ~20 residues, so the length of the bundle is ~3 nm. The N- and C-termini of the LAE are at the opposite ends of the domain, a topology consistent with its N-terminus linked to the "IQ"-motif and the C-terminus connected with the SAH rod (Fig. 1D). Therefore, the structure of the LAE indicates that the domain should provide at least ~3 nm space to each motor leg in addition to the space afforded by the "IQ"-motifs.

The packing interface of the three helices in the LAE is largely hydrophobic and the residues forming the hydrophobic core are highly conserved (Fig. 1B). The hydrophobic residues in the packing core can be classified into two clusters (Fig. 1E), and the mutation of one or more of these conserved hydrophobic residues results in severe defects in the folding of the domain. A single point mutation (I881Q) in the first cluster and double point mutations (F856Q, V860Q) in the second cluster both led to significant destabilization of the LAE folding (supplemental Fig. S2A and S2C). Interestingly, a LAE mutant containing triple point mutations in both the first and the second clusters (L853A, V870K and L884S, termed as "NM123") even did not show a clear two state folding-unfolding transition in a urea denaturation assay (supplemental Fig. S2A). Finally, the HSQC spectrum of the F865Q,V860Q-LAE mutant also revealed that the mutations have a large overall impact on the folding of the domain (supplemental Fig. S2B).

Lipid membrane-induced conformational changes of the LAE

Analysis of the molecular surface of the LAE reveals that the domain contains a positively charged surface area (Fig. 1F), which might be the motor's lipid membrane

Downloaded from www.jbc.org at Hong Kong University of Science & Technology, on September 17, 2012

contact site when the motor binds to its cargo vesicles. This prominent, positively charged surface area prompted us to test whether the domain can directly bind to lipid membranes using a sedimentation-based liposome binding assay (46). The LAE can indeed bind to liposomes prepared from bovine brain lipid extracts, albeit with an unusual concentration-dependent profile. At low concentrations of liposomes, the LAE binds robustly to the liposomes (Fig. 2A1). However, when the concentrations of liposomes were further increased, the lipid binding was unexpectedly diminished (Fig. 2A1). Extended versions of the LAE containing the C-terminal SAH domain (two fragments corresponding to residues 843-959 and 843-978, respectively) showed similar unusual concentration-dependent lipid membrane-binding patterns (Fig. 2A1&B).

To understand this intriguing lipid membrane-binding property, we resorted to simpler, NMR tractable DPC micelles to study the interaction between the LAE and lipid membranes in detail using NMR spectroscopy. At low concentrations of DPC, a selected set of the backbone amide peaks of the LAE underwent DPC concentration-dependent chemical shift changes (Fig. 2C). The mapping of these changes onto the 3D structure of the LAE showed that the residues that experienced large DPC-induced chemical shift changes are clustered and somewhat correspond to the residues forming the positively charged surface area of the domain (Fig. 2D&Fig. 1F-G). Double mutations (K851E/ R852E) in the middle of this charged surface area significantly diminished the lipid binding ability of the LAE (Fig. 2A2). We reasoned that this positively charged surface area represents the initial DPC-binding site of the LAE when the concentration of lipids is low (see below for details). Further addition of DPC resulted in the progressive broadening and eventual disappearance of the majority of the backbone amide peaks of the LAE (Fig. 2E), presumably due to the intermediate exchanges between the DPC-free and DPC-saturated conformers of the LAE. Continued addition of DPC to ~10 mM (or ~0.2 mM DPC micelles) saturated the chemical shift changes of the LAE, and concomitantly a new set of well-dispersed amide and side chain peaks was observed (Fig. 2F & data not shown), indicating that the LAE may adopt an entirely different conformation. However, the backbone amide peak distribution patterns of the LAE still indicated an α-helical conformation of the domain (Fig. 2F), which was further confirmed by the CD-based analysis of the LAE with increasing concentrations of DPC, i.e., the overall α-helical secondary structure of the domain was retained during the DPC titrations (supplemental Fig. S1C).

Analytical ultracentrifugation studies of the LAE in the presence of various concentrations of DPC showed that the sedimentation peak profile of the LAE also underwent concentration-dependent broadening, consistent with previous NMR-based observation, i.e., the DPC-free and DPC-saturated conformers of the LAE might inter-convert at intermediate concentrations of DPC (supplemental Fig. S1A&Fig. 2E). Interestingly, at the saturating concentration of DPC, the LAE appears as a symmetric and sharp peak with molecular weight indicative of a monomer (supplemental Fig, S1A), indicating that the lipid-induced conformation transition of the LAE is complete, and there is no direct interaction between the LAE and the DPC micelles. The sharp and homogenous line-widths of the backbone amide peaks of

Downloaded from www.jbc.org at Hong Kong University of Science & Technology, on September 17, 2012

the LAE in the presence of saturating DPC also support the above conclusion (Fig. 2F)). Finally, the lack of direct binding between the LAE and DPC micelles with saturating concentrations is also in line with the diminished interaction between the LAE and high concentrations of brain lipid membranes shown in Fig. 2A&B.

Taken together, the above biochemical and biophysical studies indicate that the transient contact of lipid membranes (DPC, brain liposomes, and likely the membranes of cargo vesicles of the motor) with the LAE may initiate conformational changes in the domain possibly towards the unfolded state (see below for details). Once the conformational changes are complete, the LAE tends to dissociate and diffuse away from lipid membranes, and thus may fold back for binding to lipid membranes. The whole process would be dynamic, i.e., a dynamic "kiss-and-run" interaction mode (see supplemental Fig. S4 for details).

The structural changes of the LAE in DPC micelles are reversible

Next, we asked whether the lipid membrane-induced conformational transition of the LAE is reversible, as this is an important issue in the functional switch of the motor between a cargo-vesicle transporter and a vesicle-free anchor. Again, we resorted to NMR spectroscopy, as this allowed us to monitor the conformation of the LAE with and without lipid micelles at the single amino acid resolution. We first prepared DPC/LAE mixtures by fixing the LAE at a high concentration (~1 mM) and gradually increasing the concentrations of DPC micelles. A small aliquot of the LAE/DPC mixture was withdrawn at each titration point, and this aliquot was diluted with the DPC-free buffer to mimic the gradual removal of DPC from the LAE/DPC mixture (i.e., equivalent to the reversal of the DPC titration experiment). A ^{1}H-^{15}N HSQC spectrum was recorded for each dilution mixture, and the spectrum was compared with that of the LAE (with the same DPC concentration) in the forward DPC titration experiments. This reverse titration experiment showed that the DPC-induced conformational change of the LAE is completely reversible, as indicated by the well-superimposed NMR spectra at each titration points (Fig. 3), regardless of whether the reverse titrations were started at the intermediate or fully saturated DPC-concentrations.

The structure of the LAE in the presence of lipid micelles

Next, we determined the solution structure of the LAE in the presence of saturating DPC micelles (final 20 structures with lowest energy were shown in Fig. 4A). Consistent with the CD-based analysis, the secondary structure of LAE (i.e., αA-αC) in the DPC micelles is largely retained except that the second helix (αB) is broken into two (αB1 and αB2) by a kink in the middle (Fig. 4A&5A). In contrast to the DPC-free LAE, the three α-helices of the DPC-saturated LAE do not pack with each other, which is also supported by the much narrower peak distributions of the backbone amides and side chain methyl groups (Fig. 2F & data not shown). Instead, the three α-helices adopt an open conformation, with the two termini span in a distance range of ~6-9 nm (Fig. 4A). Besides the second α-helix, another significant change of the secondary structures of the LAE induced by DPC micelles is in the first helix (αA). In DPC micelle solution, the turn between αA and αB is completely disrupted and the C-terminus of αA extends two residues (K864 and D865), leaving only two residues

Downloaded from www.jbc.org at Hong Kong University of Science & Technology, on September 17, 2012

(G866 and K867) connecting αA and αB (Fig. 4A&5A). This change somewhat restricts the conformational freedom of the first two helices (i.e., the αA helix can only rotate in a ~ 360° plane with respect to αB; Fig. 4A).

The secondary structure of αC remains largely unchanged, and interestingly, the turn between αB and αC adopts a defined conformation similar to that of the DPC-free, closed form of the LAE (Fig. 4A&5A). This defined αB/αC-turn conformation of the LAE in DPC micelles is dictated by a small hydrophobic core formed by I888, T891, M893 and I898 (as illustrated by the NOE-derived contacts among these residues, Fig. 5B&C). M893 is localized in the center of this hydrophobic core and extensively packs with other residues, and notably, it is also highly conserved in myosin VI from different species (Fig. 1). Thus, the conformational freedom between αB and αC is restricted (i.e., the αC helix can only move within a small cone with respect to αB, Fig. 4A). Finally, the surface analysis revealed that a number of positively and negatively charged residues alternately span the extended helical LAE, a type of arranging pattern that has already been implicated to stabilize the single α-helix in solution (47-48) (data not shown).

Therefore, in the presence of high concentrations of DPC, the LAE adopts an open conformation without long-range inter-helical interactions. Such lipid membrane-induced opening would certainly provide additional space to lengthen the motor "legs" (Fig. 4B). However, this open conformation is highly restrained by the defined αB/αC-turn as well as the two-residue αA/αB-linker (Fig. 4B). We hypothesize that the two inter-helix linkers (the αB/αC-turn in particular) may serve as the "memory" for the closed conformation of the LAE in aqueous solution. Upon dissociation of lipid micelles or unloading of cargo vesicles from the motor, the LAE "remembers" to revert to its compact three-helical bundle conformation (supplemental Fig. S4). This hypothesis fits well with the reversible conformational transitions of LAE between its DPC-free and DPC-saturated forms shown in the Fig. 3.

Steered molecular dynamics simulations of the LAE unfolding process

To further investigate the LAE expansion triggered by lipid membranes, we performed SMD simulations to study the unfolding process of the LAE under external forces which might be induced by the interactions with lipid membranes. The folded three-helix conformations of LAE were embedded in water boxes (large enough to include their unfolded configurations), and 6 ns of equilibration were performed to generate conformations used in SMD. During each SMD simulation, one end (the N-terminal) of LAE was harmonically constrained and another end (the C-terminal) was pulled with a spring with the spring constant of ~70 pN/nm moving with a constant velocity ~5 Å/ns. Unfolding of the LAE was observed at ~10 ns time scale under these conditions. Our simulations showed that the unfolding of WT LAE initiates from the middle of αC (Fig. 6A), which is in direct contact with the center of αA. This unfolding pathway is different from that observed by Liu et. al. (49). The discrepancy may arise from the fact that the C-terminal portion of αA was modeled as a disordered loop in the simulations by Liu et al., as unstructured C-terminal half of αA could dramatically reduce the contacts between αA and αB and thus destabilize αA. Interestingly, the

Downloaded from www.jbc.org at Hong Kong University of Science & Technology, on September 17, 2012

middle region of αA composes of a positively charged patch and is the site where lipid membranes directly interact with (Fig. 1F-G&Fig. 2D). Therefore, binding of lipid membranes to this positively charged surface may initiate the unfolding and expansion of the LAE. SMD simulations also indicate that the packing between αA and αC is somewhat intrinsically dynamic largely due to S909 in the middle of αC, as its polar hydroxyl group is unfavorable for the hydrophobic packing between αA and αC (Fig. 6A, inset). It is noted that the C-terminal half of αA is completely missing in the crystal structure of the LAE (20) (supplemental Fig. S3), possibly due to the dynamic properties of the region. To test the role of S909 for the unfolding of the LAE, we also used SMD simulations to investigate the forced unfolding of S909V mutation, which is expected to favor the hydrophobic packing of αC with αA (Fig. 6B, inset). Satisfyingly, SMD simulations indeed showed that S909V-LAE takes longer and requires larger forces to be unfolded (Fig. 6B and 6C). Consistent with the simulation, the S909V LAE also showed more tolerant to urea denaturation compared with that of the WT LAE (Fig. 6D). Taken together, both biochemical experiments and computer simulations suggest that S909 is critical in conferring myosin VI LAE to cycle between the closed helix bundle structure and the open rod-like structure in response to cargo vesicle binding.

Free MD simulations reveal the refolding tendency of the unfolded LAE

To test the stability of the extended conformation of the LAE, we next performed the free MD simulations starting with three representative conformations derived from the NMR structures in the presence of lipid micelles. In all three simulations with each lasted for ~36 ns, no significant conformational changes on each of the three helices were observed (i.e., each helix remained stable during the simulation). Interestingly, in two cases, spontaneous refolding to the helix bundle-like conformation could be observed, and the refolding appears to occur via the αB/αC region (supplemental Fig. S5). For illustration, we superimposed the simulated LAE conformations at different time points with that of the folded LAE bundle structure in aqueous solution by their respective C-terminal half of αB, and plotted the RMSD values of the αB/αC linker (supplemental Fig. S5A, the blue line) and αC (supplemental Fig. S5B, the blue line) between the simulated structures and the folded conformation of the LAE as the function of the simulation time. In one representative simulation, the αB/αC linker transits back to a conformation closely matching that of the folded LAE at ~4 ns (supplemental Fig. S5A and S5C (middle panel)). A near complete contact between αB and αC was formed at ~20 ns of the simulation time point, and this simulated refolded αB/αC conformation closely resembles that in the folded LAE in aqueous solution (supplemental Fig. S5B and S5C (lower panel)). Although a similar partial refolding tendency of αB and αC was observed in two of the three simulations, the simulation system we performed is far from the fully folded conformation of the LAE and the complete folding process definitely requires much longer simulation time to be achieved. Nevertheless, the free MD simulations of the extended LAE reveal the refolding tendency of the unfolded LAE and support our hypothesis that the αB/αC linker may serve as the "memory" for the closed conformation of the LAE.

Downloaded from www.jbc.org at Hong Kong University of Science & Technology, on September 17, 2012

MD simulations reveal the unfolding propensity induced by DPC micelles

Finally, to better understand the conformational changes of the LAE upon binding to the DPC micelle, we further performed molecular dynamics simulations of the DPC micelle-LAE system. The simulations started from three different conformations, with the interface of the LAE αA/αB, αB/αC, and αA/αC facing to the DPC micelle, respectively (supplemental Fig. S6). For each conformation, we carried out three independent initial configurations with different sides of the DPC micelle placed to interact with the LAE. Our simulations demonstrated that the αA/αB and αB/αC interface of the LAE cannot maintain stable interactions with the DPC micelle, either quickly separated (supplemental Fig. S6A-C) or tending to be separated at the end of the simulation (supplemental Fig. S6D-F). In contrast, all the simulations starting with the αA/αC interface showed the stable DPC micelle-LAE binding (supplemental Fig. S6G-I). Moreover, the binding of the LAE to the DPC micelle may further initiate the unfolding of the LAE as the separation of αA and αC was observed (supplemental Fig. S6L).

Snapshots of one representative LAE αA/αC-DPC micelle interaction simulation were shown in Fig. 7. After equilibration, the LAE formed multiple interactions with DPC molecules through the charged residues on the LAE and the hydrophilic head of DPC (Fig. 7A). These electrostatic interactions are readily attached by the surrounding water molecules, but only one such interaction was still maintained at ~70 ns of the simulation (Fig. 7E). The hydrophobic packings between the LAE and the DPC micelle were formed later (Fig. 7B-E&Fig. 1G). More interestingly, the fatty acid tail of one DPC molecule was found to directly insert into the αA/αC interface near the location where S909 resides (Fig. 7D), and the insertion became deeper with increasing the simulation time (Fig. 7E). This insertion induced the obvious separation of αA and αC as shown by the increase of the RMSD of αC when αA was aligned (Fig. 7F), thus demonstrating the unfolding propensity of the LAE in the presence of the DPC micelle.

Taken together, all these simulations confirmed that the LAE binds initially to lipid membranes via the αA/αC interface and largely mediated by the electrostatic interactions between the charged residues of the LAE and the polar head groups of lipid molecules. This initial "catch" would further induce the hydrophobic packings between the LAE and lipid molecules and the direct insertion of the hydrophobic fatty acid chain into the location of S909 (Fig. 7), which is in agreement with the data that the S909V mutant stabilizes the three-helix bundle conformation of the LAE (Fig. 6).

DISCUSSION

In this work, we found that the LAE C-terminal to the "IQ"-motif adopts a stable monomeric, three-helix bundle structure with a length of ~3 nm. Upon exposure to lipid membranes (e.g. cargo vesicles), the three helices of the LAE open to form a restrained, three-segmented rod-like structure with a size in the range of ~6-9 nm. Concurrently, the opening of the three-helix bundle provides the myosin VI's "legs" with additional flexibility (conferred by the certain conformational freedoms of the αA/αB-linker and the αB/αC-turn (Fig. 4)), thus enabling the motor to work with large and variable step sizes (Fig. 8) (18-19,30). Importantly, the conformational restraints in

Downloaded from www.jbc.org at Hong Kong University of Science & Technology, on September 17, 2012

the three helices also ensure that the entire lever arm is not completely flexible, so that the motor can respond to mechanical loads properly. Therefore, we refer to the LAE as the expandable "knee joint" of each of myosin VI's walking legs (Fig. 8). Finally, the expansion of the LAE depends on the presence of lipid membranes (i.e., when the motor is bound to cargo vesicles). The removal of lipid membranes, a process analogous to the dissociation of cargo vesicles, leads to the return of the expanded LAE into its compact three-helix bundle structure, thereby restoring the motor to its non-processive anchoring conformation (Fig. 8). Hence, the specific conformational states of the LAE encoded in its sequence are decoded by the binding of specific targets (e.g., cargo vesicles) of the motor. Nevertheless, the working model proposed for the cargo transport of myosin VI in Fig. 8 is somewhat speculative, which may need further experiments for validation in future.

Our work confirmed that the LAE indeed forms a stable helical fold in solution, which provides a length of ~3 nm for the motor's lever arm (20,34), and further revealed that the lipid membrane-induced expansion of the LAE further can extend the arm length. Thus, together with the two "IQ"-motifs N-terminal to the LAE, myosin VI can reach a step size of ~30-36 nm (Fig. 8D, walking model A), which has been well explained in the earlier studies from Sweeney's group based on the dimerization of the N-terminal region of the SAH (20-21,50). However, the work from Spudich's group demonstrated that the SAH adopts a rigid single α-helix structure (26,34), which may contribute to the large step size of myosin VI (Fig. 8D, walking model B). Thus, the "knee-joint" LAE may provide sufficient flexibilities required for the variable step size of myosin VI. Recent simulation studies of the motor suggested that a conformational transition in the converter may also contribute to the variable step size (51). Interestingly, it has been shown that the cargo-loaded myosin VI walks on actin filaments in a search-and-catch manner, with its two lever arms capable of assuming "wiggly" motions (30,52). Thus, the structural elasticity of the unfolded LAE may also provide the flexibility required by the motor, i.e., the inter-helical flexibility of the LAE in the cargo vesicle-loaded myosin VI dimer could allow the motor head to search for binding sites on actin filaments.

Recently, it was shown that the myosin VI LAE can be indeed unfolded to extend its reach during its walking process, and the dimerization of the motor (i.e., cargo-binding) is required (20). Our molecular dynamics simulations indicated that the LAE has intrinsically dynamic properties and thus may be unfolded by a relatively small amount of force (Fig. 6, cf ~1000 pN force required to unfold titin (53)). As the myosin VI medial tail (MT) closely linked to the LAE has been demonstrated to be a rigid SAH domain (Fig. 1), the dimerization of the motor by the C-terminal tail cargo-binding (12,17) or by the GCN4 dimer (33) may produce certain amount of torque force that can be transmitted by the MT to promote the unfolding/expansion of the LAE. By combining structural, biochemical, and computational studies, we here showed that lipid membranes/cargo vesicles can also induce the LAE unfolding/expansion. We envisioned that these two mechanisms for the LAE unfolding may act together, i.e., binding of the LAE to the cargo vesicles provides the second interaction site on the cargo vesicles

Downloaded from www.jbc.org at Hong Kong University of Science & Technology, on September 17, 2012

that may facilitate the force transmission from the C-terminal tail, and reciprocally, the torque force produced by the cargo-mediated dimerization of the motor may also promote the lipid membrane-induced LAE unfolding (Fig. 8). Additionally, the coupling of these two mechanisms may secure the fast response of the cargo-loading signal for myosin VI to unfold the LAE thus achieving the large and variable step sizes. Finally, given that the CBD interacts with lipid membranes/cargo vesicles and the cargo-binding-mediated dimerization converts myosin VI from a monomeric anchor to a dimeric processive transporter (Fig. 8), we also proposed that the LAE and the CBD of the motor may also function synergistically in decoding myosin VI's cargo signals via a cargo-binding-mediated dimerization coupled with the lever arm expansion mechanism.

Lipid membrane-induced conformational changes are increasingly recognized as a general molecular mechanism in controlling biological functions of both membrane and cytoplasmic proteins. It is now well known that lipid membrane elasticity (i.e. various thicknesses, curvatures and components) can perturb and reshape membrane protein structures, thereby regulating the functions of membrane proteins, such as the activities of ion-channels (see recent reviews (54-55)). Such lipid-induced conformational changes have also been observed in a number of cytoplasmic and peripheral proteins. The overall conformation of Bcl-2 can be transformed from a compact eight-helical bundle in aqueous solution into a transmembrane ion channel structure upon binding to lipid membranes (56-57). Death domains (DD) have been observed to undergo membrane-induced helix opening (58), and this conformational change might be responsible in part for the further oligomerization of DDs and the subsequent activation of the Fas-FADD death-inducing signaling complex pathway (59). In lipid membrane environments, the ALPS (ArfGAP1 lipid packing sensor) motif in a number of proteins can even transform their conformations from totally unstructured states to α-helical structures, allowing the domains to sense membrane curvatures (60-61). Together with the study described here, it is increasingly evident that lipid membranes with or without embedded proteins often function as activity regulators (or decoders of biological functions embedded in amino acid sequences) for cellular machineries by modulating their conformational properties.

REFERENCES

1. Buss, F., Spudich, G., and Kendrick-Jones, J. (2004) *Annu Rev Cell Dev Biol* **20**, 649-676
2. Sweeney, H. L., and Houdusse, A. (2007) *Curr Opin Cell Biol* **19**, 57-66
3. Buss, F., and Kendrick-Jones, J. (2008) *Biochem Biophys Res Commun* **369**, 165-175
4. Buss, F., and Kendrick-Jones, J. (2011) *Proceedings of the National Academy of Sciences of the United States of America* **108**, 5927-5928
5. Frank, D. J., Noguchi, T., and Miller, K. G. (2004) *Curr Opin Cell Biol* **16**, 189-194
6. Melchionda, S., Ahituv, N., Bisceglia, L., Sobe, T., Glaser, F., Rabionet, R., Arbones, M. L., Notarangelo, A., Di Iorio, E., Carella, M., Zelante, L., Estivill, X., Avraham, K. B., and Gasparini, P. (2001) *Am J Hum Genet* **69**, 635-640

Downloaded from www.jbc.org at Hong Kong University of Science & Technology, on September 17, 2012

7. Ahmed, Z. M., Morell, R. J., Riazuddin, S., Gropman, A., Shaukat, S., Ahmad, M. M., Mohiddin, S. A., Fananapazir, L., Caruso, R. C., Husnain, T., Khan, S. N., Riazuddin, S., Griffith, A. J., Friedman, T. B., and Wilcox, E. R. (2003) *Am J Hum Genet* **72**, 1315-1322
8. Yoshida, H., Cheng, W., Hung, J., Montell, D., Geisbrecht, E., Rosen, D., Liu, J., and Naora, H. (2004) *Proc Natl Acad Sci U S A* **101**, 8144-8149
9. Dunn, T. A., Chen, S., Faith, D. A., Hicks, J. L., Platz, E. A., Chen, Y., Ewing, C. M., Sauvageot, J., Isaacs, W. B., De Marzo, A. M., and Luo, J. (2006) *Am J Pathol* **169**, 1843-1854
10. Menetrey, J., Bahloul, A., Wells, A. L., Yengo, C. M., Morris, C. A., Sweeney, H. L., and Houdusse, A. (2005) *Nature* **435**, 779-785
11. Bryant, Z., Altman, D., and Spudich, J. A. (2007) *Proc Natl Acad Sci U S A* **104**, 772-777
12. Yu, C., Feng, W., Wei, Z., Miyanoiri, Y., Wen, W., Zhao, Y., and Zhang, M. (2009) *Cell* **138**, 537-548
13. Iwaki, M., Tanaka, H., Iwane, A. H., Katayama, E., Ikebe, M., and Yanagida, T. (2006) *Biophys J* **90**, 3643-3652
14. Park, H., Ramamurthy, B., Travaglia, M., Safer, D., Chen, L. Q., Franzini-Armstrong, C., Selvin, P. R., and Sweeney, H. L. (2006) *Mol Cell* **21**, 331-336
15. Altman, D., Goswami, D., Hasson, T., Spudich, J. A., and Mayor, S. (2007) *PLoS Biol* **5**, e210
16. Spudich, G., Chibalina, M. V., Au, J. S., Arden, S. D., Buss, F., and Kendrick-Jones, J. (2007) *Nat Cell Biol* **9**, 176-183
17. Phichith, D., Travaglia, M., Yang, Z., Liu, X., Zong, A. B., Safer, D., and Sweeney, H. L. (2009) *Proc Natl Acad Sci U S A* **106**, 17320-17324
18. Rock, R. S., Rice, S. E., Wells, A. L., Purcell, T. J., Spudich, J. A., and Sweeney, H. L. (2001) *Proc Natl Acad Sci U S A* **98**, 13655-13659
19. Nishikawa, S., Homma, K., Komori, Y., Iwaki, M., Wazawa, T., Hikikoshi Iwane, A., Saito, J., Ikebe, R., Katayama, E., Yanagida, T., and Ikebe, M. (2002) *Biochem Biophys Res Commun* **290**, 311-317
20. Mukherjea, M., Llinas, P., Kim, H., Travaglia, M., Safer, D., Menetrey, J., Franzini-Armstrong, C., Selvin, P. R., Houdusse, A., and Sweeney, H. L. (2009) *Mol Cell* **35**, 305-315
21. Sweeney, H. L., and Houdusse, A. (2010) *Cell* **141**, 573-582
22. Spudich, J. A. (2001) *Nat Rev Mol Cell Biol* **2**, 387-392
23. Mehta, A. D., Rock, R. S., Rief, M., Spudich, J. A., Mooseker, M. S., and Cheney, R. E. (1999) *Nature* **400**, 590-593
24. Walker, M. L., Burgess, S. A., Sellers, J. R., Wang, F., Hammer, J. A., 3rd, Trinick, J., and Knight, P. J. (2000) *Nature* **405**, 804-807
25. Finer, J. T., Simmons, R. M., and Spudich, J. A. (1994) *Nature* **368**, 113-119
26. Spudich, J. A., and Sivaramakrishnan, S. (2010) *Nature Reviews Molecular Cell Biology* **11**, 128-137
27. Okten, Z., Churchman, L. S., Rock, R. S., and Spudich, J. A. (2004) *Nat Struct Mol Biol* **11**, 884-887

Downloaded from www.jbc.org at Hong Kong University of Science & Technology, on September 17, 2012

28. Yildiz, A., Park, H., Safer, D., Yang, Z., Chen, L. Q., Selvin, P. R., and Sweeney, H. L. (2004) *J Biol Chem* **279**, 37223-37226
29. Nishikawa, S., Arimoto, I., Ikezaki, K., Sugawa, M., Ueno, H., Komori, T., Iwane, A. H., and Yanagida, T. (2010) *Cell* **142**, 879-888
30. Sun, Y., Schroeder, H. W., 3rd, Beausang, J. F., Homma, K., Ikebe, M., and Goldman, Y. E. (2007) *Mol Cell* **28**, 954-964
31. Shih, W. M., Gryczynski, Z., Lakowicz, J. R., and Spudich, J. A. (2000) *Cell* **102**, 683-694
32. Forkey, J. N., Quinlan, M. E., Shaw, M. A., Corrie, J. E., and Goldman, Y. E. (2003) *Nature* **422**, 399-404
33. Rock, R. S., Ramamurthy, B., Dunn, A. R., Beccafico, S., Rami, B. R., Morris, C., Spink, B. J., Franzini-Armstrong, C., Spudich, J. A., and Sweeney, H. L. (2005) *Mol Cell* **17**, 603-609
34. Spink, B. J., Sivaramakrishnan, S., Lipfert, J., Doniach, S., and Spudich, J. A. (2008) *Nat Struct Mol Biol* **15**, 591-597
35. Bax, A., and Grzesiek, S. (1993) *Acc Chem Res* **26**, 131-138
36. Kay, L. E., and Gardner, K. H. (1997) *Curr Opin Struct Biol* **7**, 722-731
37. Wuthrich, K. (1986) *NMR of proteins and nucleic acids*, John Wiley & Sons, Inc.
38. Cornilescu, G., Delaglio, F., and Bax, A. (1999) *J Biomol NMR* **13**, 289-302
39. Brunger, A. T., Adams, P. D., Clore, G. M., DeLano, W. L., Gros, P., Grosse-Kunstleve, R. W., Jiang, J. S., Kuszewski, J., Nilges, M., Pannu, N. S., Read, R. J., Rice, L. M., Simonson, T., and Warren, G. L. (1998) *Acta Crystallogr D Biol Crystallogr* **54 (Pt 5)**, 905-921
40. Koradi, R., Billeter, M., and Wuthrich, K. (1996) *J Mol Graph* **14**, 51-55, 29-32
41. Kraulis, P. L. (1991) *J. Appl. Crystallogr.* **24**, 946-950
42. Tieleman, D. P., van der Spoel, D., and Berendsen, H. J. C. (2000) *J Phys Chem B* **104**, 6380-6388
43. Phillips, J. C., Braun, R., Wang, W., Gumbart, J., Tajkhorshid, E., Villa, E., Chipot, C., Skeel, R. D., Kale, L., and Schulten, K. (2005) *J Comput Chem* **26**, 1781-1802
44. MacKerell, A. D., Bashford, D., Bellott, M., Dunbrack, R. L., Evanseck, J. D., Field, M. J., Fischer, S., Gao, J., Guo, H., Ha, S., Joseph-McCarthy, D., Kuchnir, L., Kuczera, K., Lau, F. T. K., Mattos, C., Michnick, S., Ngo, T., Nguyen, D. T., Prodhom, B., Reiher, W. E., Roux, B., Schlenkrich, M., Smith, J. C., Stote, R., Straub, J., Watanabe, M., Wiorkiewicz-Kuczera, J., Yin, D., and Karplus, M. (1998) *J Phys Chem B* **102**, 3586-3616
45. Humphrey, W., Dalke, A., and Schulten, K. (1996) *Journal of Molecular Graphics* **14**, 33-&
46. Yan, J., Wen, W., Xu, W., Long, J. F., Adams, M. E., Froehner, S. C., and Zhang, M. (2005) *EMBO J* **24**, 3985-3995
47. Peckham, M., and Knight, P. J. (2009) *Soft Matter* **5**, 2493-2503
48. Suveges, D., Gaspari, Z., Toth, G., and Nyitray, L. (2009) *Proteins* **74**, 905-916
49. Liu, Y., Hsin, J., Kim, H., Selvin, P. R., and Schulten, K. (2011) *Biophys J* **100**, 2964-2973
50. Kim, H., Hsin, J., Liu, Y. X., Selvin, P. R., and Schulten, K. (2010) *Structure* **18**,

Downloaded from www.jbc.org at Hong Kong University of Science & Technology, on September 17, 2012

1443-1449
51. Ovchinnikov, V., Cecchini, M., Vanden-Eijnden, E., and Karplus, M. (2011) *Biophys J* **101**, 2436-2444
52. Iwaki, M., Iwane, A. H., Shimokawa, T., Cooke, R., and Yanagida, T. (2009) *Nat Chem Biol* **5**, 403-405
53. Gao, M., Wilmanns, M., and Schulten, K. (2002) *Biophys J* **83**, 3435-3445
54. Phillips, R., Ursell, T., Wiggins, P., and Sens, P. (2009) *Nature* **459**, 379-385
55. Andersen, O. S., and Koeppe, R. E., 2nd. (2007) *Annu Rev Biophys Biomol Struct* **36**, 107-130
56. Minn, A. J., Velez, P., Schendel, S. L., Liang, H., Muchmore, S. W., Fesik, S. W., Fill, M., and Thompson, C. B. (1997) *Nature* **385**, 353-357
57. Schendel, S. L., Xie, Z., Montal, M. O., Matsuyama, S., Montal, M., and Reed, J. C. (1997) *Proc Natl Acad Sci U S A* **94**, 5113-5118
58. Xiao, T., Gardner, K. H., and Sprang, S. R. (2002) *Proc Natl Acad Sci U S A* **99**, 11151-11156
59. Scott, F. L., Stec, B., Pop, C., Dobaczewska, M. K., Lee, J. J., Monosov, E., Robinson, H., Salvesen, G. S., Schwarzenbacher, R., and Riedl, S. J. (2009) *Nature* **457**, 1019-1022
60. Bigay, J., Casella, J. F., Drin, G., Mesmin, B., and Antonny, B. (2005) *Embo J* **24**, 2244-2253
61. Drin, G., Casella, J. F., Gautier, R., Boehmer, T., Schwartz, T. U., and Antonny, B. (2007) *Nat Struct Mol Biol* **14**, 138-146

Acknowledgements: We thank Anthony Zhang for critical reading of the manuscript. This work was supported by grants from the National Major Basic Research Program of China (2011CB910503), the National Natural Science Foundation of China (31070657, 31190062 and 31070827), the Knowledge Innovation Program of the Chinese Academy of Sciences (KSCX2-YW-R-154 and KSCX2-EW-J-3), and the Research Grants Council of Hong Kong to M.Z. (664009, 660709, 663610, HKUST6/CRF/10, SEG_HKUST06 and AoE/M-04/04). We would also like to thank the Computer Network Information Center of Chinese Academy of Sciences (DeepComp 7000), Shanghai Supercomputer Center (Magic Cube), and National Supercomputing Center in Tianjin (Tianhe) for computational resources. M.Z. is a Senior Fellow of the Institute for Advanced Study at HKUST.

FOOTNOTES

Coordinates:

The atomic coordinate of myosin VI LAE in aqueous solutions has been deposited in the Protein Data Bank with accession code 2LD3.

Abbreviations: LAE, lever arm extension; CaM, calmodulin; "IQ"-motif, a short sequence starting with Ile and Gln for calmodulin binding; SAH, single α-helix; CBD, cargo-binding domain; SMD, steered molecular dynamics; NMR, nuclear magnetic resonance; HSQC, heteronuclear single quantum coherence; NOE, nuclear Overhauser effect; DPC,

Downloaded from www.jbc.org at Hong Kong University of Science & Technology, on September 17, 2012

dodecylphosphocholine; CD, circular dichroism; RMSD, the root-mean-square deviation.

FIGURE LEGENDS

Figure 1: Solution structure of the LAE. (A) Domain organization of myosin VI. The LAE domain is a region between the neck (one "IQ"-motif and a unique insertion) and the SAH domain. CBD stands for the Cargo-Binding Domain of the motor. **(B)** Sequence alignment of the LAE from different species. The identical residues are colored in red, and highly conserved residues are in green. The residue numbers and the secondary structures are marked on the top, and the residues responsible for the three-helix bundle packing core are highlighted by yellow dots at the bottom. **(C)** Stereo-view showing the backbones of 20 superimposed NMR-derived structures of LAE. The N- and C-termini of the protein are labeled. **(D)** Ribbon diagram of a representative NMR structure of LAE. The length of the three-helix bundle is ~3 nm. **(E)** Stereo-view showing the hydrophobic packing core of the bundle. Two hydrophobic clusters are highlighted by two dashed ovals. The residues from the N-terminus of αA (L843, V846 and L849), the C-terminus of αB (I881, L884, M885 and I888), the N-terminus of αC (I898, Y902 and L905) and the αB-αC loop (M893) form the first cluster (Cluster I); the residues from the C-terminus of αA (L853, F856, V860 and L863), the N-terminus of αB (V870, I874 and L877) and the C-terminus of αC (L912 and L916) form the second cluster (Cluster II). **(F)** Surface charge potential analysis of LAE showing a positively charged surface area, composed of K845, K850, K851, R852 and K855 from αA, and R895 and K920 from αC. In this drawing, the positive charge potential and negative charge potential are represented in blue and red, respectively. **(G)** Surface analysis of LAE showing a positively charged cluster in αA and a hydrophobic patch between αA and αC. In this drawing, the positively charged residues, negatively charged residues, hydrophobic residues and others are colored in blue, red, yellow and gray, respectively.

Figure 2: Lipid membrane-induced conformational changes of the LAE. (A-B) Sedimentation-based liposome binding assay showing the lipid binding properties of the LAE (843-933) (A1), the LAE with double mutations (KR/EE) (A2), and the LAE with C-terminal SAH domain (843-959 and 843-978) (B). Fractions labeled with "S" or "P" denote proteins present in supernatants or pellets after centrifugation respectively. The data showed the biphasic lipid membrane binding properties of all three LAE-containing fragments of myosin VI. **(C)** The overlay plot of ^{1}H,^{15}N-HSQC spectra of LAE with increasing concentrations of DPC at the initial stage of the DPC titration. The peaks undergoing large chemical shift changes are marked by black arrows. **(D)** Mapping of the DPC binding-induced chemical shift changes onto the 3D structure of LAE, showing that the positively charged surface area experienced the largest shift changes. The scale of the shift changes is shown at the right of the panel. **(E-F)** The ^{1}H,^{15}N-HSQC spectra of LAE in the presence of ~4 mM (approximately half-saturated, panel E) and ~10 mM (fully saturated, panel F) of DPC. The boxed region in panels C, E and F are used to highlight the obvious spectral changes during the titration. The insert in panel F shows the chemical shift changes of N876 during the entire titration process.

Figure 3: DPC-induced conformational changes of the LAE are reversible. (A, C and E)

Downloaded from www.jbc.org at Hong Kong University of Science & Technology, on September 17, 2012

The $^{1}H,^{15}N$-HSQC spectra of the LAE (recorded with protein concentration ~1 mM) at three increasing concentrations of DPC indicated in the figure. **(B)** The overlay plot of $^{1}H,^{15}N$-HSQC spectra of an aliquot of the LAE/DPC mixture from panel A with ~10 times dilution (red, final DPC concentration ~1.0 mM) with that of LAE in the forward titration with approximately same DPC concentration (black). The near complete overlay of the two spectra indicated that upon the removal of DPC (from panel A to B), the conformation of the LAE can be fully reverted to its closed state. (**D**) The overlay plots of HSQC spectra of an aliquot of the LAE/DPC mixture from panel B with ~12 times dilution (red, final DPC concentration ~1.6 mM) with that of the LAE in the forward titration with approximately same DPC concentration (black). (**F**) The overlay plots of spectra of an aliquot of the LAE/DPC mixture from panel C with ~25 times dilution (red, final DPC concentration ~1.2 mM) with that of the LAE in the forward titration with approximately same DPC concentration (black). The data illustrate that the DPC-induced conformational transition of the LAE is fully reversible. The acquisition times were lengthened accordingly in order to obtain sufficient signal to noise ratios for the HSQC spectra of the diluted samples

Figure 4: Overall structure of the LAE in DPC micelles. (A) Ribbon diagram of the 20 superimposed (using the second helix, αB, residue 868-891) NMR-derived structures of the LAE in DPC micelles. The N- and C-termini of the protein are labeled. The figure shows that the first helix (αA, residue 846-865) can rotate in a ~360° plane with respect to αB, and that the third helix (αC, residue 895-922) can only move within a small-angled cone with respect to αB. It is not clear whether the kink in the middle of αB may be related to the function of LAE. **(B)** A structural model containing the motor domain (orange), the "IQ" motifs in complex with the Ca^{2+}-CaM (magenta) and the apo-CaM (cyan), and the LAE in the closed conformation (green) and in a variety of open conformations (purple). The opening of the LAE may provide both the space and the flexibility for myosin VI to walk with large and variable steps.

Figure 5: Structural changes of the LAE induced by DPC micelles. (A) The combined $^{13}C\alpha/^{13}C\beta$ chemical shift index plot of the LAE in both aqueous and DPC solutions. In this plot, the secondary chemical shift of each amino acid residue is expressed as the $^{13}C\alpha$ secondary shift minus the $^{13}C\beta$ secondary shift with a smoothing window of 3. The secondary structures of the LAE in both aqueous and DPC solutions are shown at the top of each graph. The regions undergoing large secondary structural changes are indicated by red and cyan dash lines. **(B)** Stereo-view showing the hydrophobic core of the αB/αC-turn. The side chains of each core-forming residue are drawn in explicit atomic representations. **(C)** Selective strips of ^{13}C-seperated NOESY spectrum showing the observed NOEs between the residues in the αB/αC-turn.

Figure 6: Identification of the unfolding initiation site of the LAE. (A-B) SMD simulations of the unfolding process of the wild type (WT) LAE (A) and the S909V LAE (B). For each system, two separated independent simulations were performed. SMD forced unfolding was started with the fully equilibrated structures and the unfolding snapshots of one simulation were shown as representative for both WT (A) and S909V (B) systems. The

Downloaded from www.jbc.org at Hong Kong University of Science & Technology, on September 17, 2012

LAE equilibrated structures (0 ns, purple) were compared with the corresponding conformations (gray) building from the NMR structures. Representative snapshots (with simulation time marked) are selected to demonstrate various statuses of the simulation process (from the top to the bottom with the time increasing). The initiation unfolding site of the LAE near S909 is located in the middle of αC. The interfaces between αA and αC surrounding S909 suggest that the S909V-mutant would have a more tightly packed core than the WT (Inset, right-top figures of each panel). **(C)** The force-extension curve of the SMD simulations for WT (red and magenta) and S909V (blue and cyan). The unfolding of the S909V LAEs needs larger force (~400 pN) than the WT ones (~300 pN). **(D)** Urea-denaturation profiles (the ellipticity values at 222 nm were plotted as the function of the urea concentration) of the WT LAE and the S909V mutant. The S909V LAE is more tolerant to urea, as the unfolding transition of the LAE dramatically shifts to the higher concentrations of urea.

Figure 7: MD simulations of the DPC micelle-induced LAE unfolding. (A-E) Snapshots of a representative MD simulation showing the interaction between the LAE αA/αC interface and the DPC micelle with simulation time indicated. Basic, acidic, non-charged polar and hydrophobic LAE residues ~5 Å close to the DPC micelle are shown in blue, red, green, and orange, respectively. Residue S909 is highlighted and marked. DPC molecules ~5 Å close to the LAE are shown in balls and sticks. For clarity, DPC molecules are only shown in the snapshot at ~0 ns and ~70 ns. The specific DPC molecule, which directly inserts into the αA/αC interface, is shown in purple. **(F)** Time course of the RMSD of αA (black) and αC (blue) when αA was aligned, indicating the separation of αC from αA.

Figure 8: A schematic model illustrating the myosin VI-mediated cargo transport. Prior to cargo vesicle binding, myosin VI exists in a closed conformation with the C-terminal cargo-binding domain (CBD) folding back to interact with the motor domain via a yet unknown mechanism (A). The folded-back conformation keeps myosin VI in its monomeric state, in which the LAE adopts a globular closed conformation. Upon the binding of cargo vesicles, the CBD is released from its sequestration by the motor domain. The binding of the cargo adaptor (e.g. Dab2) converts the myosin VI into a dimer, a step essential for its processive walking on actin filaments. In parallel, binding of cargo vesicles to the motor (and the dimerization of the motor) leads to the expansion of LAE from a three-helix bundle to an extended, partially flexible rod-like structure in a "kiss-and-run" manner (B-C). Currently, there are two models for myosin VI's stepping. In the first model, the N-terminal end of the SAH can be dimerized and the unfolded LAE adopts an extended structure (D, walking model A). In the second model, the SAH forms a rigid single α-helix structure, which may also contribute to the large step size of myosin VI (D, walking model B). In these two models, the unfolded LAE may offer both the space and the flexibility needed for the large and variable step sizes of myosin VI and likely functions as the "knee-joint" of the motor. Notably, the arm angles of myosin VI between these two walking models are significantly different. Finally, after the cargo unloading, myosin VI may be converted back to its closed conformation (A). As such, the motor is reset for its next functional cycle.

Downloaded from www.jbc.org at Hong Kong University of Science & Technology, on September 17, 2012

Figure 1

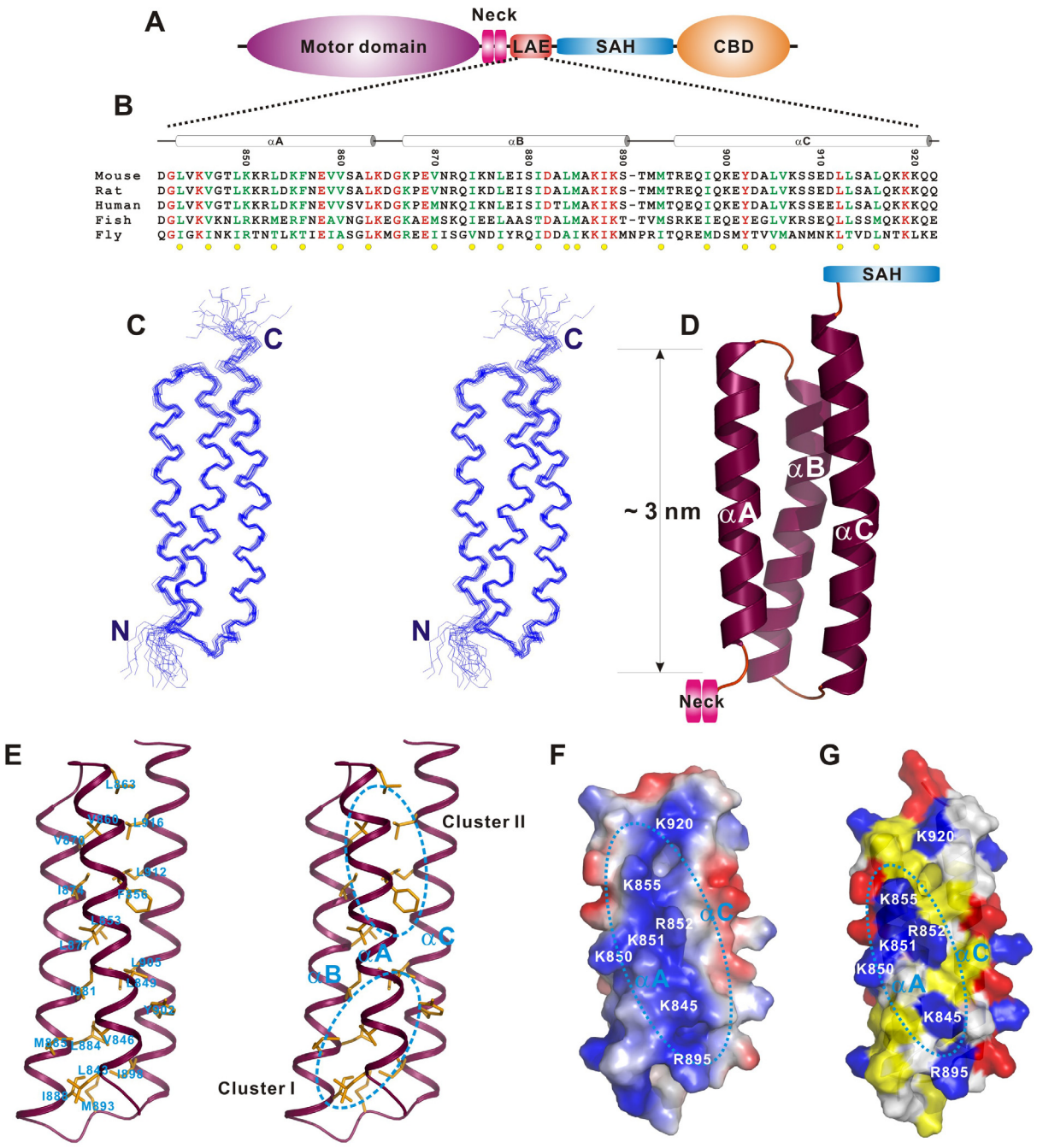

Downloaded from www.jbc.org at Hong Kong University of Science & Technology, on September 17, 2012

Figure 2

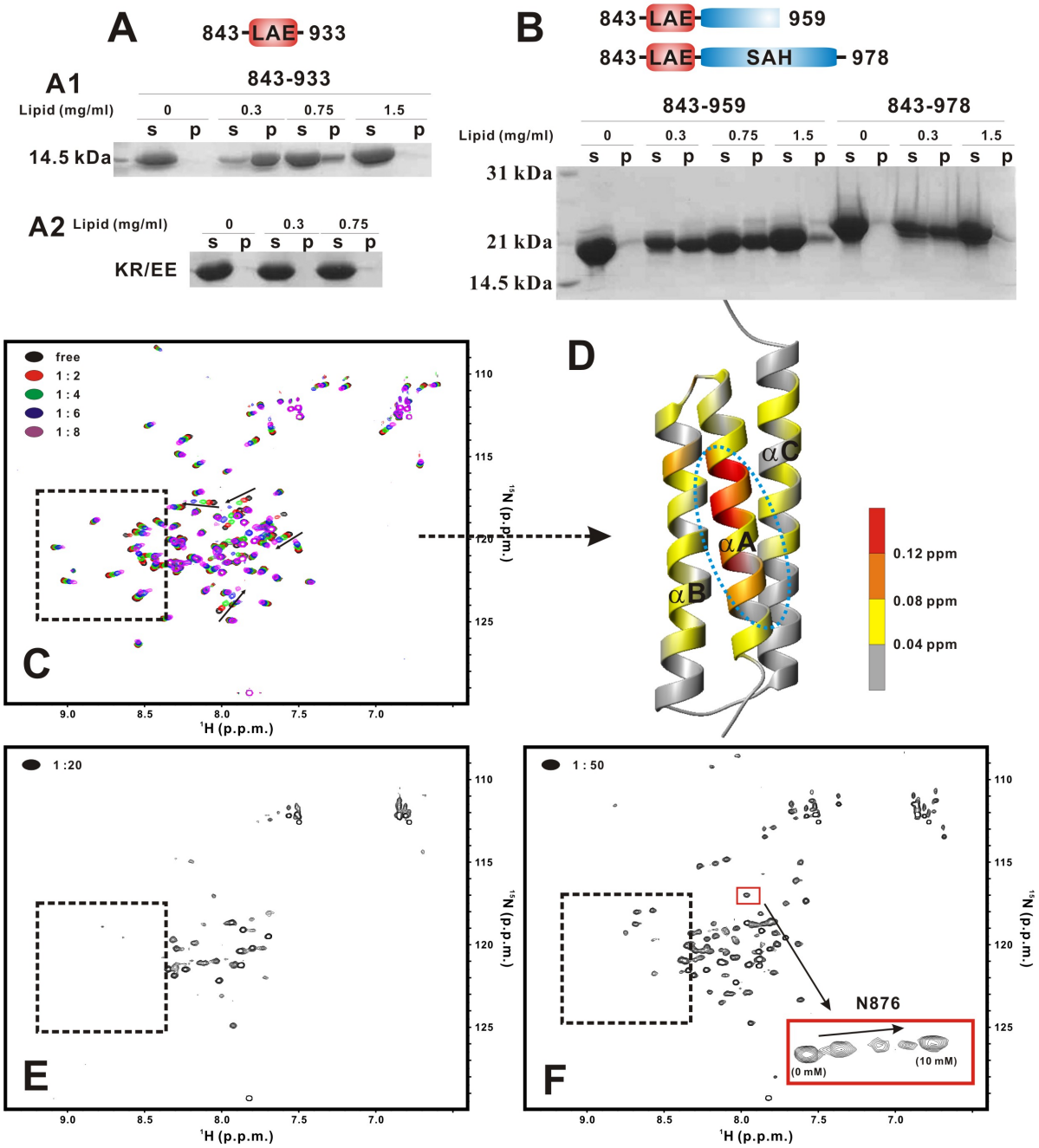

Downloaded from www.jbc.org at Hong Kong University of Science & Technology, on September 17, 2012

Figure 3

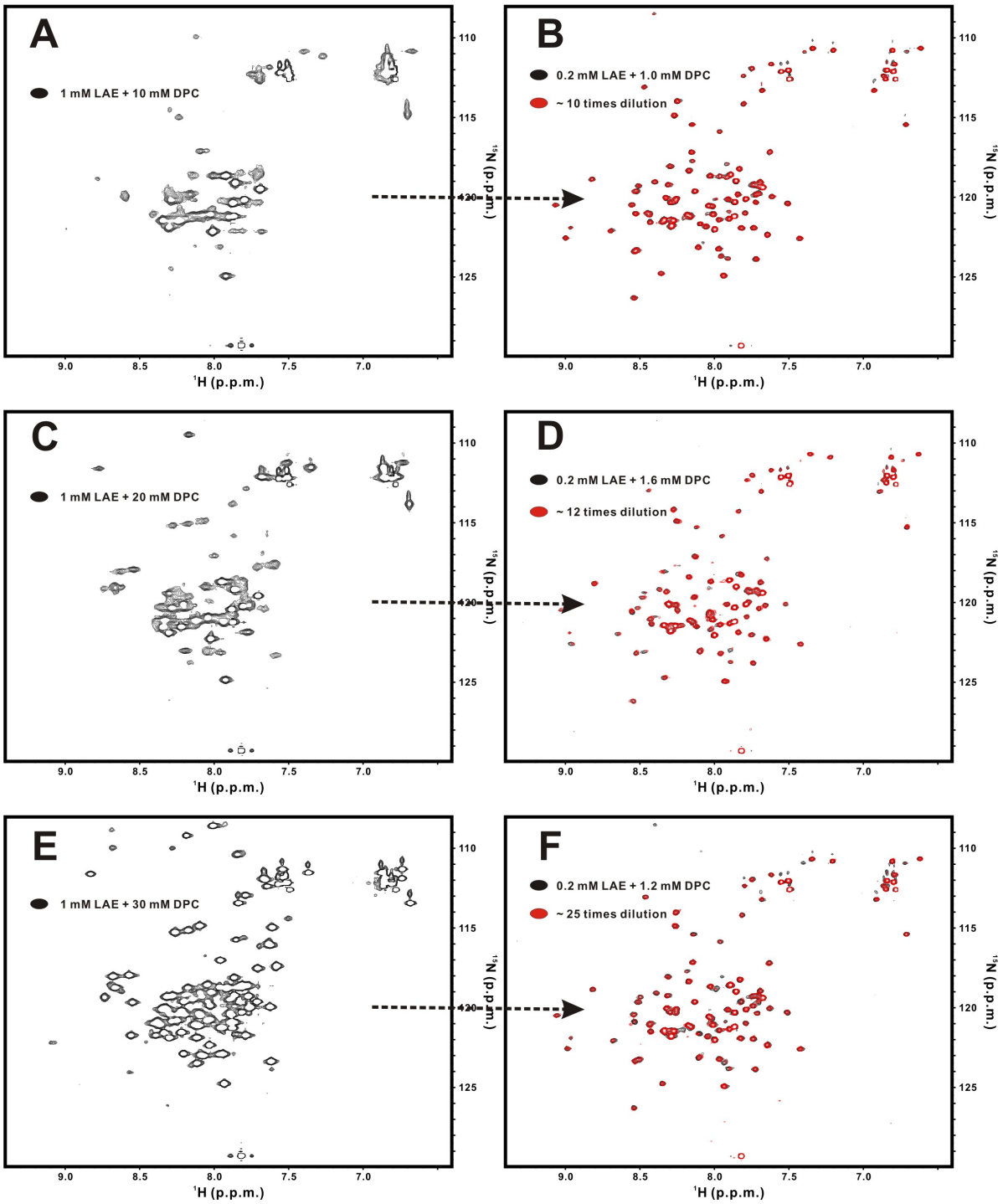

Downloaded from www.jbc.org at Hong Kong University of Science & Technology, on September 17, 2012

Figure 4

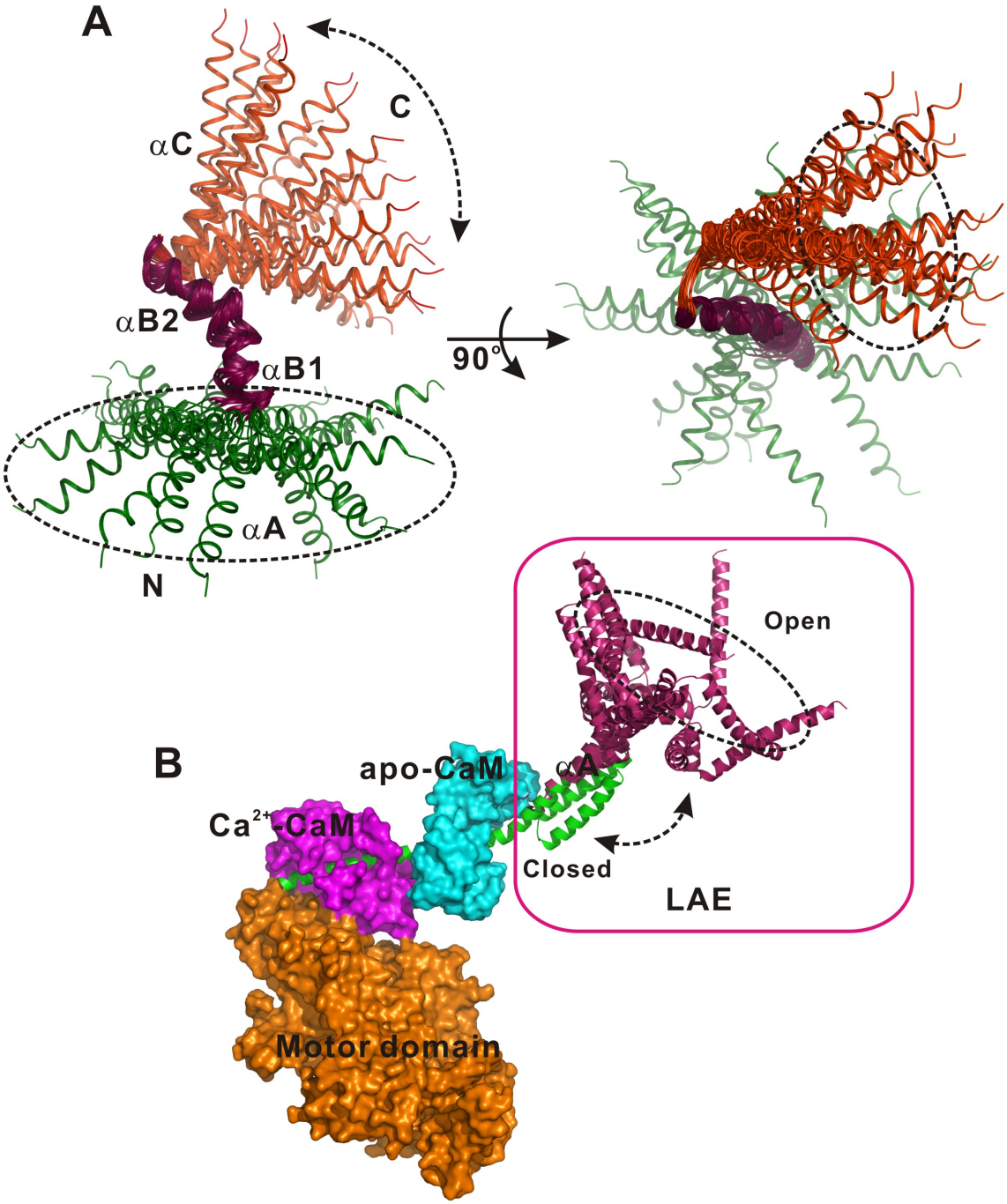

Downloaded from www.jbc.org at Hong Kong University of Science & Technology, on September 17, 2012

Figure 5

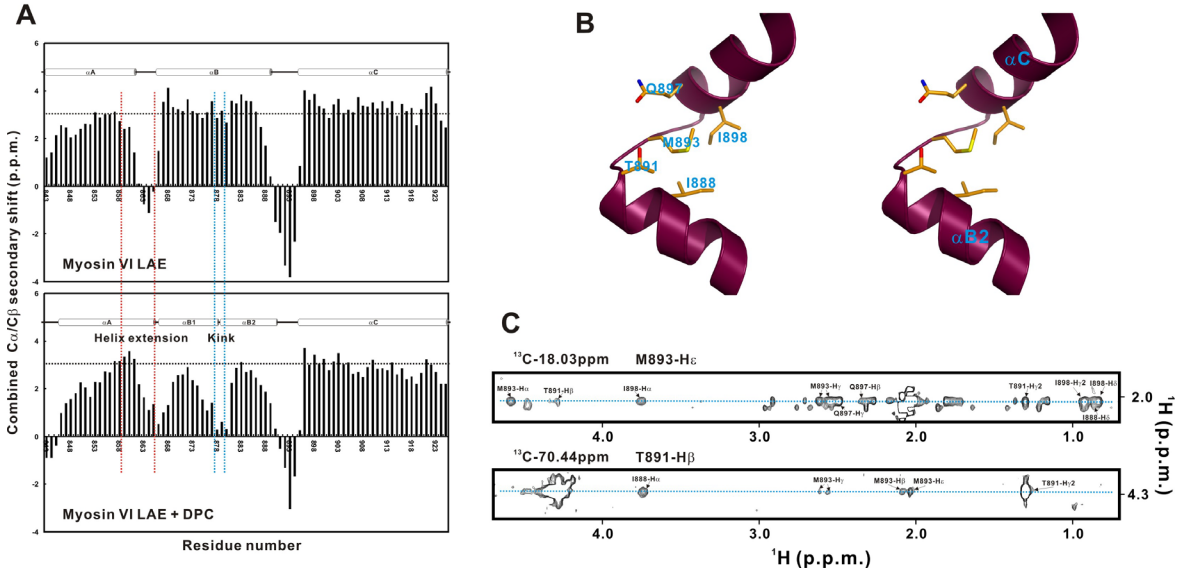

Downloaded from www.jbc.org at Hong Kong University of Science & Technology, on September 17, 2012

Figure 6

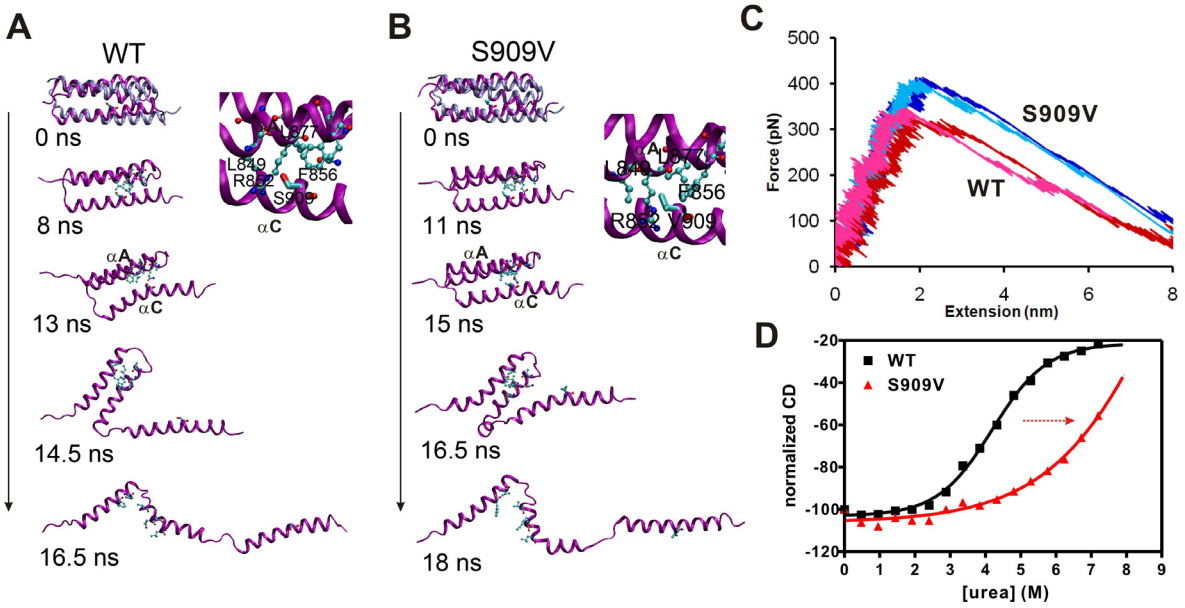

Downloaded from www.jbc.org at Hong Kong University of Science & Technology, on September 17, 2012

Figure 7

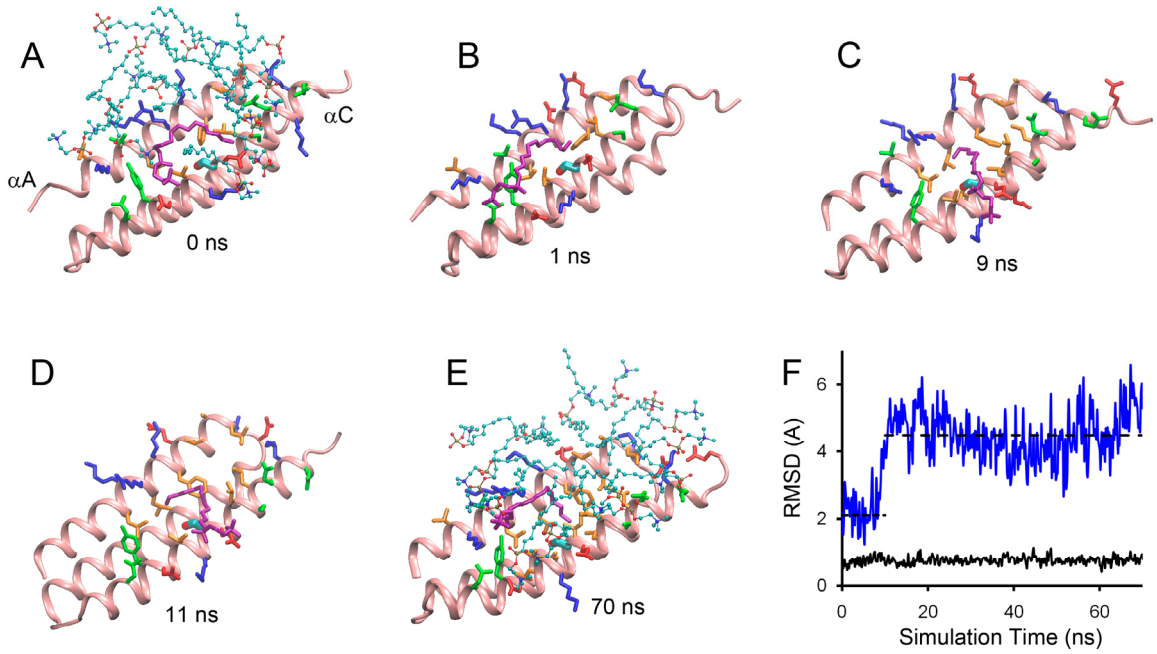

Downloaded from www.jbc.org at Hong Kong University of Science & Technology, on September 17, 2012

Figure 8

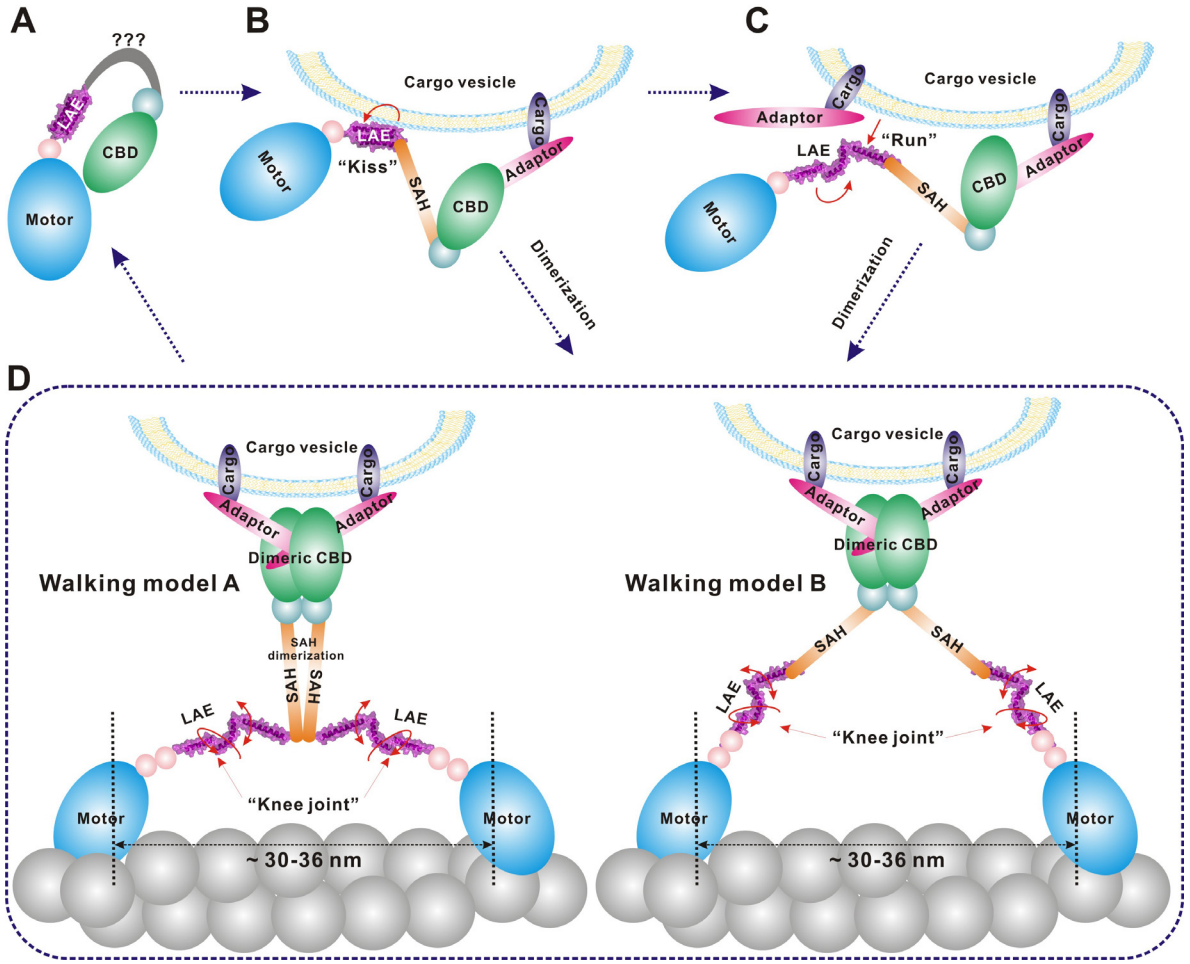

Downloaded from www.jbc.org at Hong Kong University of Science & Technology, on September 17, 2012